

# Tuning Range Comparison Between Different Planar Inductors Layouts on PCB

<sup>1,2</sup>Sinda Kaziz

<sup>1</sup>METS research group, École nationale d'ingénieurs de Sfax, Université de Sfax, Sfax, Tunisia

<sup>2</sup>Faculté des sciences de Monastir, Université de Monastir, Tunisia  
[sinda.kaziz@fsm.u-monastir.tn](mailto:sinda.kaziz@fsm.u-monastir.tn)

<sup>1,4</sup>Fares Tounsi

<sup>1</sup>METS research group, École nationale d'ingénieurs de Sfax, Université de Sfax, Sfax, Tunisia

<sup>4</sup>Institut supérieur d'informatique et de mathématiques de Monastir, Université de Monastir, Monastir 5019, Tunisia  
[fares.tounsi@isimsf.rnu.tn](mailto:fares.tounsi@isimsf.rnu.tn)

<sup>1,2</sup>Bilel Maamer

<sup>1</sup>METS research group, École nationale d'ingénieurs de Sfax, Université de Sfax, Sfax, Tunisia

<sup>2</sup>Faculté des sciences de Monastir, Université de Monastir, Tunisia  
[bilel.maamer@fsm.u-monastir.tn](mailto:bilel.maamer@fsm.u-monastir.tn)

<sup>3</sup>Laurent A. Francis

<sup>3</sup>SMALL Research Group, ICTEAM Institute, Place du Levant 3, Université catholique de Louvain, Louvain-la-Neuve, Belgium

[laurent.francis@uclouvain.be](mailto:laurent.francis@uclouvain.be)

<sup>3</sup>Thibault Delhaye

<sup>3</sup>SMALL Research Group, ICTEAM Institute, Place du Levant 3, Université catholique de Louvain, Louvain-la-Neuve, Belgium

[thibault.delhaye@uclouvain.be](mailto:thibault.delhaye@uclouvain.be)

<sup>3</sup>Denis Flandre

<sup>3</sup>SMALL Research Group, ICTEAM Institute, Place du Levant 3, Université catholique de Louvain, Louvain-la-Neuve, Belgium

[denis.flandre@uclouvain.be](mailto:denis.flandre@uclouvain.be)

**Abstract**—This paper aims at comparing the tuning range of three different planar inductor layouts built on a Printed Circuit Boards (PCB), namely the spiral inductor, the non-spiral inductor, and the meander inductor. Initially, we identify the equivalent electric model for the three inductors. All models are validated theoretically by analytical equations, by simulation through Sonnet software<sup>®</sup>, and also by measurements. For the same surface occupancy, the spiral inductor presents the higher inductance value, while the non-spiral inductor has the higher quality factor and self-resonant frequency. The tunability range is investigated by placing a shielding metal plate above for all PCB inductors. The inductance value is reduced, when the air gap between the metal plate and the inductance decreases. In addition, results demonstrated that the spiral inductor has the higher range, with a variation of more than 90%, followed by the non-spiral inductor. The meander one showed a change less than one-tenth of the spiral inductor.

**Keywords**—passive component, PCB spiral inductor, tuned inductor.

## I. INTRODUCTION

Over the last decades, planar passive components have played a crucial role in the development of the electronics industry. They have been used in numerous electric and electronic equipments, in a wide area of applications, such as telecommunications infrastructure, industrial electronics, automotive electronics, servers, some data processing equipments, etc. [1] Notably, the Printed Circuit Board (or PCB) inductor is gaining attraction for wireless power transfer applications due to their various advantages over conventional inductors such as batch fabrication, low cost, manufacturability on flexible substrates, simplicity and durability. Passive devices, including capacitors and inductors, could be classified into two types: fixed and variable. With technological progress, variable inductor components are playing essential roles in RF circuits, voltage-controlled oscillator (VCO), passive filter, radio transmitters, power amplifiers, reconfigurable impedance matching networks, etc. [2] Tuning or varying the inductor component value can be achieved through four methods: (i) the inductive coupling tuned inductor is based mainly on the adjustment of mutual inductance between the primary and

secondary windings of the split total inductor [3], (ii) the magnetic core tuned inductor is based on a magnetic core conductor which permeability can be changed when applying a magnetic field [4], (iii) a discretely-tuned inductor is often realized using micro relays [5] or micro-switches [6] to vary the effect of the effective inductor length, (iv) the metal shielding tuned (MST) inductor is realized using a movable metal plate [7], so that inductance variation results from the change of the inductor magnetic flux. This paper will examine adjustable inductors patterned on PCB. Hence, the goal is to compare the tuning range of three different PCB planar inductors through metal shielding.

Initially, we start with a lumped-element model comprehension of three different types of planar square inductors built on PCB, namely the spiral, the meander, and the non-spiral inductors. This theoretical study will be validated through the measurements of the characteristics over a frequency range up to 10 MHz in order to accurately analyze the inductor properties. Lastly, we will be interested in comparing metal shield tuning capability between these three investigated planar inductors.

## II. PLANAR PCB INDUCTORS MODEL EXTRACTION

The three investigated inductors are made with 17 $\mu$ m-thick copper conductive lines sketched on a FR4-type Board. For all drawn shapes, the inductor is specified by the number of turns  $n$ , the segment width  $w$ , the spacing between two consecutive turns  $s$ , the inner diameter  $d$ , and the outer diameter  $D$  (Fig. 1). The latter was set identical, equal to 20 mm, for all inductance layouts. A variety of approaches for modeling planar inductors on PCB by an equivalent circuit have been reported in the past few years [8][9]. Fig. 2 shows the most common lumped-element equivalent model of a planar inductor. In this model,  $L_s$  represents the series inductance of the traces,  $R_s$  the series resistance of the conductive lines, and  $C_s$  the inter-strips stray-capacitance [8].

The performance of an inductor is mainly determined by its quality factor  $Q$ , which affects the circuits and/or devices in which it is implemented. The quality factor is defined as the ratio between the stored magnetic energy  $E_{stored}$  and the dissipated energy  $E_{loss}$  over one signal cycle as:

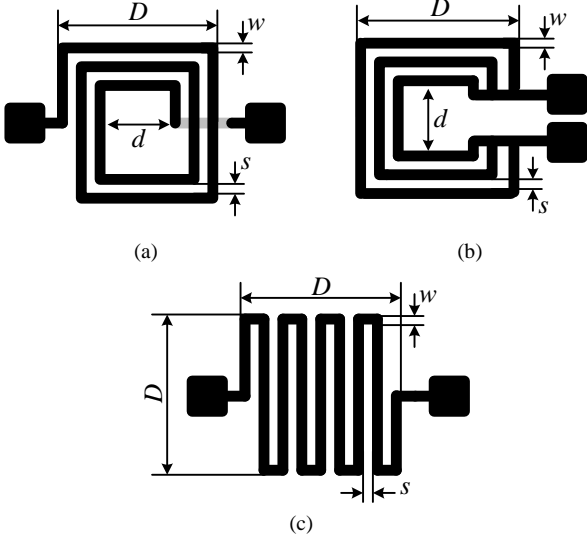


Fig. 1: Conceptual sketches of the 3 investigated inductor layouts: (a) Spiral, (b) Non-spiral, and (c) Meander.

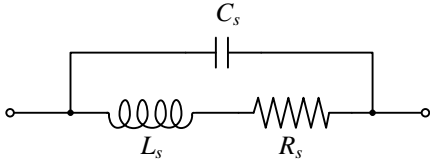


Fig. 2: Common electrical lumped-elements model of the planar inductor.

$$Q = 2\pi \frac{E_{\text{stored}}}{E_{\text{loss}}} = -\frac{\omega (C_s R_s^2 - L_s + C_s L_s^2 \omega^2)}{R_s} \quad (1)$$

The given  $Q$ -factor expression, which is frequency dependent, takes into account the parasitic capacitance but not the losses into the substrate. Generally, the operating frequency of the inductor is chosen when the  $Q$  factor is at its highest peak, before starting the decay down to zero at the self-resonant frequency (SRF) [10]. The model parameters of the different inductor layouts will be extracted in the following subsections.

#### A. Square spiral inductor

The square planar spiral inductor is the most popular in radio-frequency applications due to the high achievable inductance values per unit of wire length. This feature is reached thanks to its rolled layout design approaching the standard ones (Fig. 1a), and which promotes contribution of positive mutual inductance between neighboring conductors in the resulting inductance value. In such a layout, the winding requires at least two metal layers to connect the

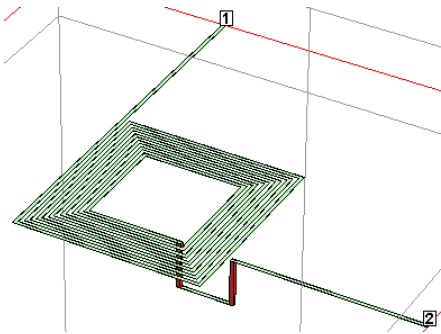


Fig. 3: Perspective view of the spiral inductor drawn with Sonnet® software.

Table 1: Square spiral inductor dimensions.

$n$	$W$	$S$	$D$	$d$	$L$
6.5	0.4 mm	0.4 mm	20 mm	10.4 mm	384 mm

Table 2: Comparison of inductance values calculated from different formulas.

Method	Inductance $L_s$ ( $\mu\text{H}$ )
Bryan [11]	1.12
Greenhouse [11]	1.11
Rosa [11]	1.09
Cranin [11]	1.35
Terman [11]	0.84
Monomial [11]	0.74
Simulation result	1.1
Experimental result	1

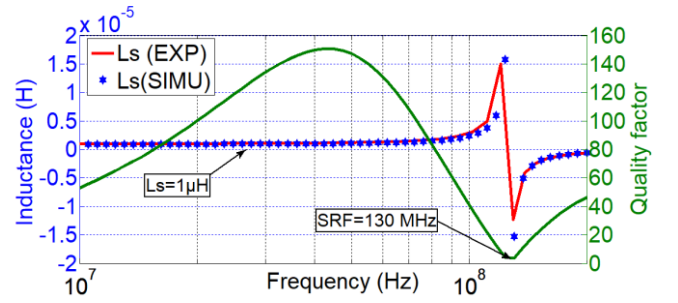


Fig. 4: Simulated inductance and quality factor of the spiral inductor.

internal terminal. Initially, analytical extraction of the inductor parameters will be carried out by simulation with Sonnet® Software.

Fig. 3 shows a perspective view of the 3D structure of the investigated planar spiral inductor with the dimensions listed in Table 1. The variation of the simulated inductance and quality factor versus frequency, from 10 MHz to 200 MHz, are depicted in Fig. 4. From this graph, three operating regions can be identified, depending on the inductance sign versus frequency. Region I presents the useful band wherein the inductance value remains positive and relatively constant. Region II is called the transition region in which the inductance increases at a faster rate and then becomes negative with a capacitive behaviour in Region III. The frequency at which the inductance value crosses zero is called the self-resonant frequency, or SRF. Lastly, in region III, the parasitic inter-strips capacitance dominates, and hence the device should not be used within that region. The self-resonant frequency is expressed as:

$$SRF = \frac{1}{2\pi\sqrt{L_s C_s}} \quad (2)$$

From Fig. 4, it can be seen that the simulated quality factor  $Q$  increases up to 150 at 42 MHz, then slowly drops up to zero at the self-resonant frequency which equals 130 MHz.

Theoretically, several expressions have been proposed to estimate the square spiral planar inductance value according to their geometrical parameters [11]. Referring to dimensions given in Table 1, inductance values are calculated from different closed-form expressions, in order to evaluate and compare their accuracy. Table 4 collects

assessment from these different analytic formulas for evaluating their outputs versus simulation. We can affirm that all results are in a reasonably fair agreement, and the relative error does not exceed 35%.

The series resistance of the planar spiral inductor can be calculated using:

$$R_s = \frac{\rho l}{w \delta (1 - e^{-\frac{t}{\delta}})} \quad (3)$$

where  $\rho$  is the copper resistivity [ $\Omega\text{m}$ ],  $l$  the overall length of the spiral inductor,  $w$  and  $t$  the width and the thickness of the copper conductor trace, respectively, and  $\delta$  the metal skin depth given by:

$$\delta = \sqrt{\frac{2\rho}{2\pi f \mu_0 \mu_r}} \quad (4)$$

The DC series resistance  $R_s$  was analytically computed to be  $1.08 \Omega$  (frequency independent part), which is in an admissible agreement with the simulated value of  $0.95 \Omega$ .

The parasitic capacitance  $C_s$  in planar inductors, whose influence appears toward high frequencies, is given by [12]:

$$C_s = \frac{2l\epsilon_0}{\pi} \ln\left(\frac{w + \frac{s}{2}}{\frac{s}{2}}\right) \quad (5)$$

where  $\epsilon_0$  is the electric vacuum permittivity ( $8.85 \text{ pF}\cdot\text{m}^{-1}$ ). This stray capacitance was analytically evaluated to be  $2.7 \text{ pF}$ .

To verify the accuracy of the simulated equivalent inductor model, we extracted real parameters from measurements. An integrated parameter analyzer Keithley 4200-SCS (from  $100 \text{ kHz}$  to  $10 \text{ MHz}$ ) is connected to the inductor on board shown in Fig. 5. The effects of the extra conductive traces, connecting the main PCB inductor to BNC connectors, are removed with de-embedding using separate open and short structures. The test equipment was calibrated in the concerned operating frequency band, i.e. from  $100 \text{ kHz}$  to  $10 \text{ MHz}$ , and its noise uncertainty verified to be insignificant [12]. The measured impedance is drawn in Fig. 6, and then compared with the simulated data of the inductor. The best fitting procedure using Matlab<sup>®</sup> was applied to extract model parameters from the measurement, and the obtained circuit was simulated in Pspice<sup>®</sup>. The values extracted from measurements are  $L_s=1 \mu\text{H}$ ,  $R_s=0.95 \Omega$  and  $C_s=1.6 \text{ pF}$  (the latter is calculated from the resonance frequency). From Fig. 6, we can see that the inductor model is in good agreement with the measured data, with a relative error less than 10%.

### B. Meander inductor

The meander inductor is very common because of its simple production process on one layer (Fig. 1c). Indeed,

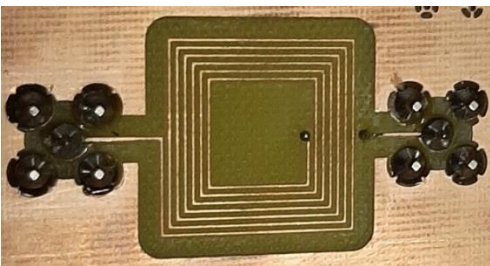


Fig. 5: The spiral inductor on PCB.

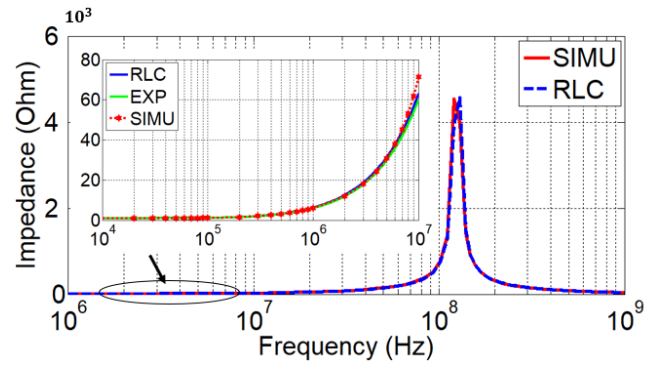


Fig. 6: Measured and simulated equivalent impedance of the spiral inductor.

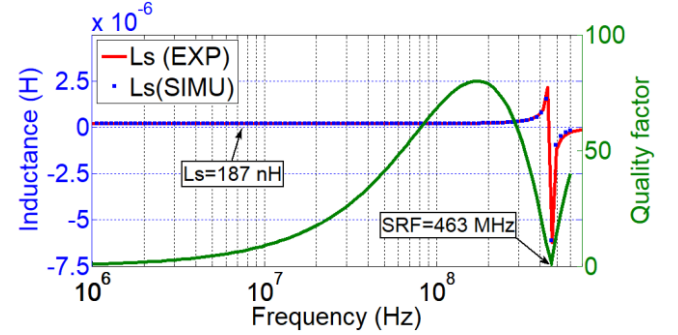


Fig. 7: Simulated inductance and quality factor of the meander inductor.

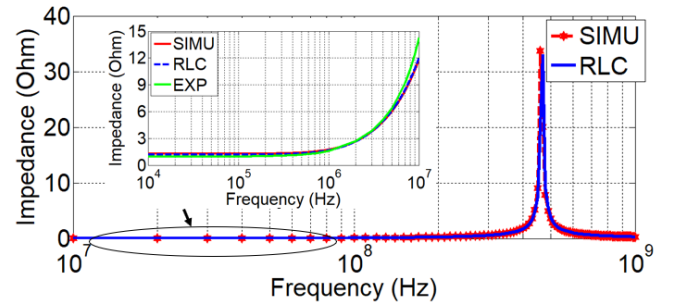


Fig. 8: Measured and simulated equivalent impedance of the meander inductor.

there is no need for an internal metal pad contact as in two-level spiral inductors. This saves two photolithography masks and simplifies the technological process. Moreover, in meander inductor, the current vectors of adjacent tracks are opposite, causing a negative mutual inductance. Therefore, its inductance value is about 3-8 times lower (depending on dimensions) compared to the value achieved with a spiral geometry of the same effective track length. The fabricated structure has dimensions of  $20 \text{ mm} \times 20 \text{ mm}$ ,  $0.4 \text{ mm}$ -track width and 25 meanders. Similar to the spiral inductor, the meander can be modeled by a parasitic capacitor  $C_s$  in parallel with a series inductance  $L_s$  and a series resistor  $R_s$ . The inductance  $L_s$  can be calculated by [8]:

$$L_s = 0.002l \left[ \ln\left(\frac{2l}{w+h}\right) + \left(\frac{w+t}{3l}\right) + 0.50049 \right] \quad (6)$$

where  $l$  is the length of the segment of the meander inductor. Fig. 7 presents the evaluation of the inductance and the quality factor over frequencies. The extracted value of the inductance from Sonnet<sup>®</sup> Software simulation is  $190 \text{ nH}$ , while the measured one is  $185 \text{ nH}$ . The analytic expression

given in Eq. 6 yields 192 nH. So, we can confirm that results are in a good agreement with a relative error less than 10%. The SRF of the designed meander inductor is 463 MHz. The series resistance  $R_s$  was evaluated analytically to be 1.3  $\Omega$ , measured at 0.99  $\Omega$ , and simulated from Sonnet to be 1.3  $\Omega$ . The measured parasitic capacitance was estimated from SRF to be 0.62 pF, versus 0.63 pF from simulation. Fig. 8 illustrates the measured equivalent impedance of the meander inductor, which is in good agreement with the experimental and the Spice simulated LRC circuit.

### C. Planar non-spiral inductor

Planar inductances are classified into spiral and non-spiral types. In the spiral inductance, the center turn has contact to lead outside using a via connection, which requires another metal layer. The non-spiral type has both contact pads on the same level, as shown in Fig. 1b, thus only one metal layer during fabrication is required. [13]. Moreover, non-spiral inductors are advantageous in term of energy consumption as their resistance is lower than the spiral one. The low resistance is achieved due to the short-circuited turns' configuration which causes a non-homogeneous distribution in the magnetic field. The reason behind is due to the asymmetrical current division between the turns of the inductor since they are interconnected as a set of short-circuited parallel conductors. Hence, the innermost turn has the least resistance, so the majority of the input current flows through it which makes the magnetic field maximum in the vicinity. So, the resistance of the turns increases gradually towards the outer turns, which in turn leads to a decrease in the magnetic field towards the outer turns. The analytic expression for calculating the inductance of a square planar non-spiral inductor  $L_s$  with a single turn is given by [15]:

$$L_s = \frac{2\mu D}{\pi} \left[ \ln\left(\frac{4D}{w+h}\right) + 0.894 \frac{w+h}{4D} - 0.660 \right] \quad (7)$$

The series resistance  $R_s$  of one inductor spiral can be calculated using Eq. 3 divided by the number of parallel turns, and similarly to calculate the total inductance. The parasitic capacitance  $C_s$  of the interspace between segments can be approximately calculated using:

$$C_s = \frac{\pi \epsilon h D}{s} \quad (8)$$

Fig. 9 and Fig. 10 show, respectively, the evaluation of the inductance, the quality factor and the equivalent impedance of the inductor over the frequency. The extracted value of the inductance from Sonnet simulation was 24 nH, while the measured one is 22 nH. The analytic expression gives 20 nH, which is in a good agreement with others.

### D. Inductor Layouts comparison

Inductors designed in PCB process on FR4 substrates have the capability of providing an inherently higher inductance value compared to silicon-based ones. Consequently, their  $Q$ -factor is much higher than silicon inductors which is typically lower than 25. In this subsection, characteristics of the three investigated inductors types, implemented on the same PCB area of 20 mm  $\times$  20 mm, are compared. Table 2 gathers obtained results, where we can note that the spiral inductor presents the

Table 2: Comparison of the parameters of the inductors implemented on an identical area.

parameters geometries	Spiral inductor	Meander inductor	Non-spiral inductor
$L_s$	1.10 $\mu\text{H}$	0.187 $\mu\text{H}$	20 nH
$R_s$	0.95 $\Omega$	1.3 $\Omega$	60 m $\Omega$
$C_s$	1.62 pF	0.63 pF	1.06 pF
$Q$	150	82	352
SRF	130 MHz	463 MHz	1.085 GHz

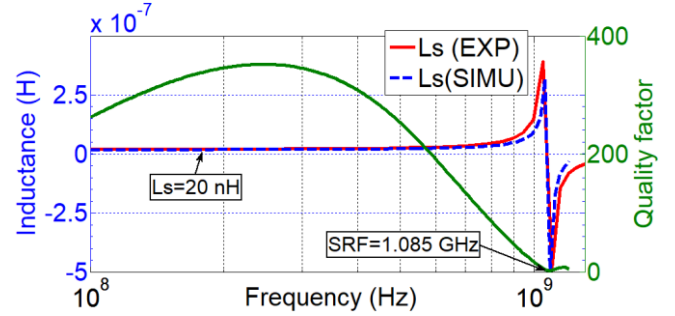


Fig. 9: Variation of the inductance of the non-spiral inductor.

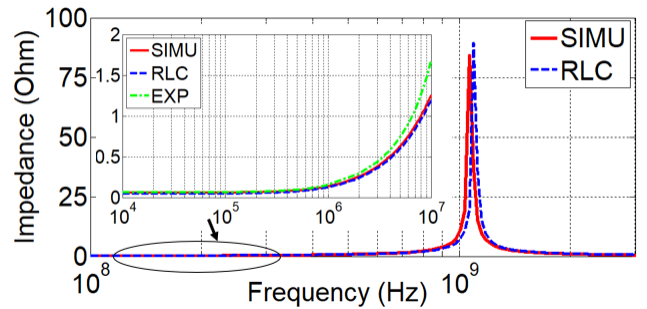


Fig. 10: The equivalent impedance of the non-spiral inductor.

higher inductance value, whereas the non-spiral inductor presents the lower one. The highest SFR and quality factor are for the non-spiral inductor because of the lowest inductance and resistance values (see Eq. 2). Lastly, the meander can be fabricated on a single conductor layer, but its resistivity is the highest, and hence the  $Q$  factor is the lowest. Despite its very low inductance, the non-spiral inductor shows interesting properties in terms of SFR, quality factor and resistivity.

## III. TUNING INDUCTORS RANGE COMPARISON

### A. Tuning inductors theory

Tuning the spiral inductor will be based on the metal shielding tuning (MST) method. The mechanism is realized using a movable metal plate, and the equivalent model is shown in Fig. 11a. It consists of two parts: the planar spiral inductor and the shielding metal plate above. The mechanism can be described as follows: when the moveable plate approaches the inductor, this will cause a change in the magnetic flux lines which will penetrate the shielding metal plate. Based on Lenz-Law, a counteractive magnetic field will be induced, and the shielding metal plate will lessen the original magnetic field. This will in turn reduce the inductor stored magnetic energy, and hence the inductance value will be decreased. Therefore, when the metal plate moves down and gets closer to the spiral, the distance  $d$  decreases and the

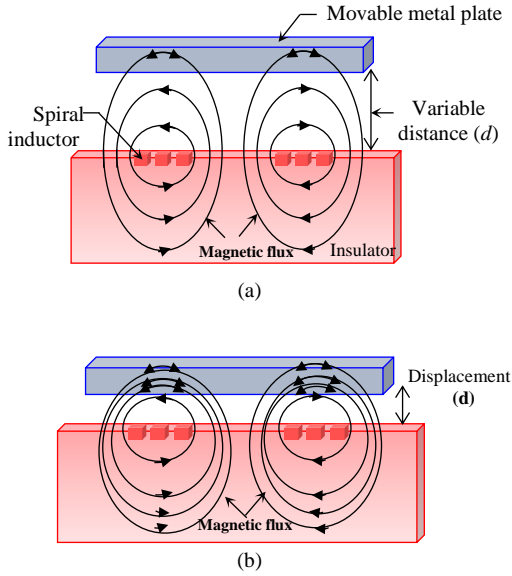


Fig. 11: Mechanism of the tuned inductor with magnetic flux tuning (a) Normal position, (b) Actuated position.

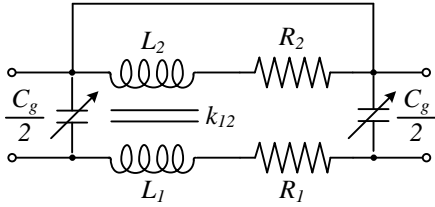


Fig. 12: Equivalent circuit model of the metal shielding tuned spiral inductor.

penetrating magnetic flux increases, as shown in Fig. 11b [11]. Fig. 12 presents the equivalent circuit model of the tuned inductor, which is different from the traditional one. In this figure,  $L_1$  is the series inductance of the spiral inductor,  $L_2$  is the equivalent inductance of the shielding metal plate,  $R_1$  is the series resistance of the spiral inductor,  $R_2$  is the equivalent resistance of the shielding metal,  $C_g$  is the parasitic capacitance between the spiral inductor and shielding metal plate and  $k_{12}$  is the equivalent coupling coefficient between the movable shielding metal plate and the spiral inductor, given by:

$$k_{12} = \frac{M_{12}}{\sqrt{L_1 \cdot L_2}} \quad (9)$$

where  $M_{12}$  is the mutual inductance between coil 1 and coil 2. In this proposed model,  $k_{12}$  and  $C_g$  are functions of the distance  $d$ , while the other parameters are not [14].

### B. Tuning inductors range

In order to compare the tunability range of the different fabricated inductor layouts, the distance  $d$  between the spiral inductor and the shielding copper plate is varied from 100  $\mu\text{m}$  to 500  $\mu\text{m}$ . In practice, a 100  $\mu\text{m}$ -thick sheet paper (having a permittivity of 2.36 and loss tangent of  $\sim 0.06$ ) is sandwiched between the inductor and the copper plate. The latter is tightened slightly to evacuate the air on both sides of the paper. For higher thicknesses, the appropriate number of sheets is inserted to obtain the desired separation gap. Fig. 13 and Fig. 14 show, respectively, the variation of the inductance and the quality factor of the spiral inductor over frequency for different distances. As expected, the inductance value increases as  $d$  increases because the

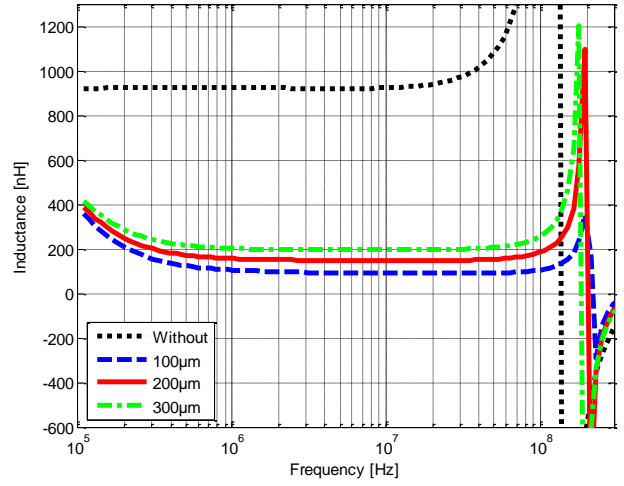


Fig. 13: Inductance versus frequency of the tuned spiral inductor for different distance  $d$ .

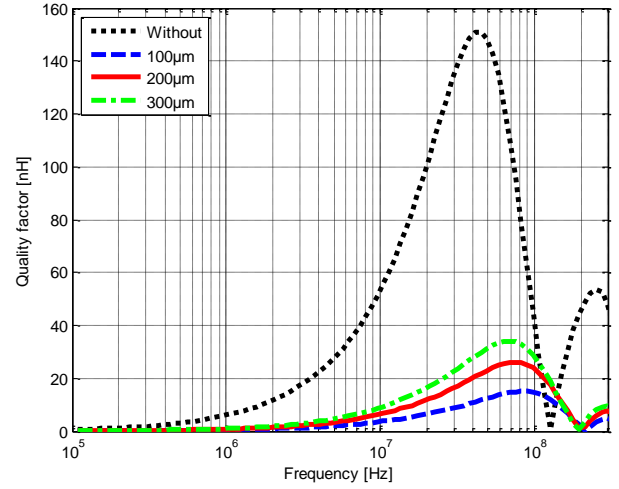


Fig. 14: Quality factor versus frequency of the tuned spiral inductor for different distance  $d$ .

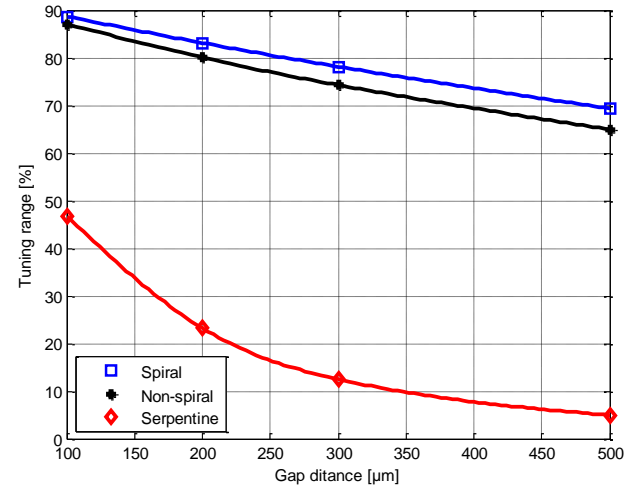


Fig. 15: Variation of the tuning range for different inductance layouts @ 1MHz as a function of the distance  $d$ .

amount of magnetic flux that penetrates the metal plate decreases, as shown in Fig. 13. Fig. 14 depicts that the quality factor also increases as  $d$  increases. Indeed, the shielding metal plate penetrates as well the electric field of the spiral inductor. Therefore, a parasitic capacitance

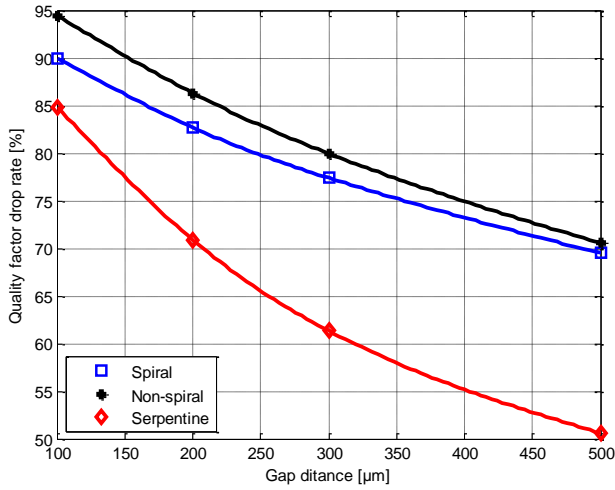


Fig. 16: Variation of the quality factor drop rate for different inductance layouts @1MHz as a function of the distance  $d$ .

appears between the inductor traces and the metal plate, which participates in the degradation of the inductor behavior. The parasitic capacitance depends on the distance  $d$  between the spiral inductor and the metal plate. Moreover, since the quality factor approximately varies with inductance, we can affirm that the decrease of the quality factor is caused additionally by the decrease of inductance. The self-resonance frequency increases slightly as  $d$  decreases, and this is a consequence of the decrease in  $L_s$ . To compare inductance tunability, we can define the tuning range factor (TR) as the percentage of inductance variation between the initial and tuned values. A point worth emphasizing is that the tunability is better attained for frequencies approaching SRF, and is very low at low frequencies as shown in Fig. 13. The tuning range is calculated with [10]:

$$TR = \frac{L_0 - L_t}{L_0} \quad (10)$$

where  $L_0$  and  $L_t$  are the initial and the tuned inductor values, respectively. This characteristic is a significant factor, particularly for variable inductors. Fig. 15 and Fig. 16 present respectively the variation of the tuning range TR of the inductance and the quality factor of different geometries as a function of the metal plate distance from the inductor at the frequency of 10MHz. It is worth noting that the spiral inductance represents the higher TR which is about 90% at  $d=100 \mu\text{m}$  for the inductance and 90% for the quality factor while the meander inductance has the lower. Non-spiral inductor presents performances which are very close to that of the spiral inductor.

#### IV. CONCLUSION

In this paper, we present a comparison between the characteristics of three different planar inductor layouts drawn on PCB: namely the spiral inductor, non-spiral inductor and meander inductor. The different parameters of an RLC equivalent electric model were analytically estimated for each one, and next confirmed by simulations and experiments. Because of its layout, the spiral inductor

presents the higher inductance; however, the non-spiral inductor presents the higher SRF and quality factor. Lastly, the tuning inductor mechanism via metal shield was investigated. The separation distance between the spiral inductor and the metal plate was varied from  $100\mu\text{m}$  to  $500\mu\text{m}$ . The tuning range was the higher, more than 90%, for the spiral inductor closely followed by the non-spiral one.

#### ACKNOWLEDGEMENT

This work was carried out with support provided from the Fonds de la recherche scientifique (FNRS), Belgium under the framework of the European project Horizon 2020 named "CONVERGENCE" in the field of science and technology.

#### REFERENCE

- [1] B. Sasic, M. Damjanovic, L. Zivanov, C. Zlebic, and N. Blaz, "Design and modelling of two-layer inductor on PCB substrate," 39<sup>th</sup> International Spring Seminar on Electronics Technology (ISSE), pp. 515–520, 2016.
- [2] M. Zolog, D. Pitica, and O. Pop, "Characterization of spiral planar inductors built on printed circuit boards," 30<sup>th</sup> International Spring Seminar on Electronics Technology (ISSE), pp. 308–313, 2007.
- [3] I. Zine-El-Abidine, M. Okoniewski, and J. G. McRory, "RF MEMS tunable inductor using bimorph microactuators," International Conference on MEMS, NANO and Smart Systems, pp. 436–437, 2005.
- [4] J. Salvia, J. A. Bain, and C. P. Yue, "Tunable on-chip inductors up to 5 GHz using patterned permalloy laminations," IEEE International Electron Devices Meeting, 2005. IEDM Technical Digest., pp. 943–946, 2005.
- [5] S. Zhou, X.-Q. Sun, and W. N. Carr, "A micro variable inductor chip using MEMS relays," International Solid State Sensors and Actuators Conference (Transducers'97), vol. 2, pp. 1137–1140, 1997.
- [6] P. Park, C. S. Kim, M. Y. Park, S. Do Kim, and H. K. Yu, "Variable inductance multilayer inductor with MOSFET switch control," IEEE Electron Device Letters, vol. 25, no. 3, pp. 144–146, 2004.
- [7] Y. Yin, Z. Liu, J. Zheng, L. Chen, S. Wu, S. Wang, Z. Yan, and X. Pan, "The Effects of Position on the Wear Debris Detection with Planar Inductor," Sensors, vol. 19, no. 22, pp. 4961, 2019.
- [8] G. Haobijam and R. P. Palathinkal, "Design and analysis of spiral inductors," Springer, 2014.
- [9] A. B. Islam, S. K. Islam, and F. S. Tulip, "Design and optimization of printed circuit board inductors for wireless power transfer system," Circuit and System, vol. 4, no.2, pp. 237–244, 2013.
- [10] O. F. Hikmat and M. S. M. Ali, "RF MEMS inductors and their applications—A review," Journal of Microelectromechanical Systems, vol. 26, no. 1, pp. 17–44, 2016.
- [11] M. K. Kazimierczuk, "High-frequency magnetic components". John Wiley & Sons, 2009.
- [12] F. Tounsi, D. Flandre, L. Rufer, and L.A Francis, "Performances Evaluation of On-chip Large-Size Tapped Transformer for MEMS applications," IEEE Transactions on Instrumentation and Measurement, online on February 2020.
- [13] M. Biglarbegian, N. Shah, I. Mazhari, and B. Parkhideh, "Design considerations for high power density/efficient PCB embedded inductor," 3<sup>rd</sup> IEEE Workshop on Wide Bandgap Power Devices and Applications (WiPDA), pp. 247–252, 2015.
- [14] D.-M. Fang, X.-H. Li, Q. Yuan, and H.-X. Zhang, "Design, simulation, and characterization of variable inductor with electrostatic actuation fabricated by using surface micromachining technology," IEEE transactions on electron devices, vol. 57, no. 10, pp. 2751–2755, 2010.
- [15] S. Krishnapriya, H. Chandrakar, R.S. Komaragiri, and K.J. Suja, "Performance analysis of planar microcoils for biomedical wireless power transfer links," Sādhanā, Vol 44, No. 187, July 2019.